Minimum Distortion Point Tracking

Jason Poon, *Member, IEEE*, Brian B. Johnson, *Member, IEEE*, Sairaj V. Dhople, *Member, IEEE*, and Seth R. Sanders, *Fellow, IEEE*

***Abstract*—This article introduces the notion of *minimum distortion point tracking (MDPT)*: a control strategy where switching waveforms are optimally phase shifted to minimize aggregate ripple power for networks of dc–dc converters that are connected in series or parallel at the input or output. In a sense, MDPT generalizes the ubiquitous concept of interleaving in balanced systems to a broad class of asymmetric series- or parallel-connected dc–dc converters. For networks of up to one hundred interconnected power converters, MDPT demonstrates a one to two order of magnitude reduction (-14 to -22 dB) in distortion power. We present and experimentally verify three algorithms that can dynamically solve the MDPT optimization problem on a network of three input-parallel connected dc–dc buck converters handling 1.8 kW. The experimental results illustrate an up to 3.06$\times$ reduction in the peak-to-peak ripple of the parallel-side bus voltage and convergence close to an optimal steady-state solution in 5 ms.**

***Index Terms*—DC–DC power conversion, optimization methods, power conversion harmonics.**

I. Introduction

SERIES- and parallel-connected dc–dc converters are ubiquitous in many power electronics systems, such as point-of-load conversion systems, dc microgrids, and integrated circuits with multiple on-die voltage domains [2]–[4]. In balanced systems, symmetric phase shifting (i.e., interleaving) is widely used due to numerous benefits that can be obtained through control, including a scaling of the effective switching frequency by the number of converters, a net ripple amplitude reduction, and associated improvements in power quality and conducted electromagnetic interference (EMI) [5]–[8]. However, in general, asymmetries from independent source or load connections or from nonidealities in converter passive and active components may arise in networks of dc–dc converters that are connected in series or parallel at the input or output (e.g., in microgrids, point-of-load conversion systems, and voltage regulation modules). In such networks, it remains an open question whether phase shifting can yield benefits similar to interleaving in symmetric systems. Indeed, while interleaving is a particular operating regime where switching waveforms for a system of N converters are phase shifted $360^\circ/N$ apart, in asymmetric systems, the optimal phase shifting may conceivably be entirely different.

This article introduces *minimum distortion point tracking* (MDPT), which generalizes the notion of interleaving in balanced systems to a broader class of asymmetric networks of dc–dc converters that are connected in parallel or series at the input or output. We present the concept of the *minimum distortion point* (MDP), which establishes a first principles limit on the ac ripple power (or equivalently, the distortion) that is attainable with phase shifting for a network of interconnected dc–dc converters. The MDP is defined as the phase shift for switching waveforms across the converters that minimizes the aggregate distortion in an ℓ_p-norm sense. Minimization of this ac power is desirable in that it is precisely this quantity that determines the minimum filtering needed to satisfy a maximum ripple constraint. Using this definition, we develop three practical algorithms for MDPT. In particular, these algorithms are real-time optimization methods that nudge the system toward the MDP. Each MDPT algorithm is experimentally verified on a network of three input-parallel connected dc–dc buck converters handling a total power of 1.8 kW. The results illustrate peak-to-peak ripple reductions up to 3.06$\times$ and convergence close to an optimal steady-state solution in 5 ms. Moreover, numerical analysis on networks of up to 100 interconnected buck converters indicate that MDPT can enable a one to two orders of magnitude reduction (-14 to -22 dB) in distortion power relative to distortion power obtained with uncoordinated converter operation.

A variety of methods have been proposed in the literature to minimize the ripple or harmonic components in individual and interconnected power converters. Perhaps most well-known is harmonic elimination or reduction pulsewidth modulation (PWM) schemes [9]–[12]. Unlike MDPT, these techniques apply to a single power converter and focus on static, open-loop PWM that eliminates specific harmonics in the output waveform. "Asymmetric" interleaving techniques for multiphase dc–dc converters have been explored in a number of works. In [13], the authors propose and analyze scenarios in which N converters are identically phase separated θ°, where $\theta \neq 360^\circ/N$. In [14], the authors present a strategy to arbitrarily phase shift multiphase

Manuscript received September 7, 2019; revised December 28, 2019; accepted February 12, 2020. Date of publication February 21, 2020; date of current version June 23, 2020. This work was supported in part by the US Department of Energy (DOE) Office of Energy Efficiency and Renewable Energy administered by the Oak Ridge Institute for Science and Education (ORISE), Oak Ridge Associated Universities (ORAU) under DOE Contract DE-SC0014664. This paper was presented in part at the 19th IEEE Workshop on Control and Modeling for Power Electronics (COMPEL), Padova, Italy, June 25, 2018 [1]. Recommended for publication by Associate Editor Prof. Michael (GE) A. E. Andersen. *(Corresponding author: Jason Poon.)*

Jason Poon is with the Department of Electrical Engineering, Stanford University, Stanford, CA 94305 USA (e-mail: jason.poon@stanford.edu).

Brian B. Johnson is with the Department of Electrical and Computer Engineering, University of Washington, Seattle, Washington 98195 USA (e-mail: brianbj@uw.edu).

Sairaj V. Dhople is with the Department of Electrical and Computer Engineering, University of Minnesota, Minneapolis, Minnesota 55455 USA (e-mail: sdhople@umn.edu).

Seth R. Sanders is with the Department of Electrical Engineering and Computer Sciences, University of California, Berkeley, California 94305 USA (e-mail: seth.sanders@berkeley.edu).

Color versions of one or more of the figures in this article are available online at http://ieeexplore.ieee.org.

Digital Object Identifier 10.1109/TPEL.2020.2975613

dc–dc converters to minimize the sum of the first harmonic of the aggregate ripple component. MDPT fundamentally differs from both of these techniques since it considers arbitrary phase shifts across multiple power converters and optimally minimizes a norm of the *total harmonics* of the ripple component. Moreover, while the techniques in [13] and [14] utilize precomputed phase shifting parameters or look-up-tables, MDPT dynamically generates and optimizes the phase spacing as a function of the network, the operating point, and the input conditions. In other work, optimal programmed PWM schemes have been proposed that spread the spectral energy from switching circuit waveforms across a higher number of harmonic frequencies (thus reducing the peak spectral components) [15]. In a similar direction, randomized PWM schemes have been proposed to minimize peak spectral components by utilizing a random frequency or phase modulation [16], [17]. However, both techniques do not reduce the total undesired harmonic energy, but rather spread it away from concentrated discrete frequencies. In addition, only individual power converters are considered, and networks of interconnected power converters are not addressed.

Compared to existing literature, MDPT is novel in four distinct ways.

1. It is designed for multiple dc–dc power converters with arbitrary topologies connected in parallel or series at the input or output; in particular, it considers: a) different converter topologies, b) different interconnection architectures, including converters connected in series or parallel and radial, loop, or network systems, and c) network models capturing parasitics and line impedances.
2. It establishes a first principles limit on the minimum ac ripple power that is attainable with phase shifting.
3. It considers phase shifts across multiple power converters that are not necessarily equal.
4. It dynamically generates and optimizes the phase spacing scheme in a closed-loop fashion as a function of the network, the operating point, and the input conditions.

The remainder of this article is organized as follows. Section II presents the mathematical principles of the MDP. Section III presents a conceptual overview of MDPT methods and the unconstrained optimization problem that seeks the phase shifting across a generalized network of power converters that will bring the system to the MDP. Algorithms for implementing MDPT based on the gradient method, the nonlinear Gauss–Seidel (NL–GS) method, and a metaheuristic optimization scheme are presented in Sections IV, V, and VI, respectively. Experimental results on a network of three input-parallel connected dc–dc buck converters validate the performance of each algorithm. Section VII presents analysis and comparisons of the characteristics of each algorithm with respect to computational complexity, convergence speed, decentralization of control, and the optimality of the steady-state solution. Section VIII concludes the article.

II. Defining the Minimum Distortion Point (MDP)

In this section, we define the MDP in a precise mathematical sense. We do so in the context of a system of N dc–dc buck converters operating in continuous conduction mode at periodic steady state with identical switching frequencies, f_s, and connected in parallel at the input (see Fig. 1). As discussed previously, this setup is merely to fix ideas and is without loss of generality. Indeed, the MDP can be defined for any network of dc–dc converters that are connected in series or parallel at the input or output.

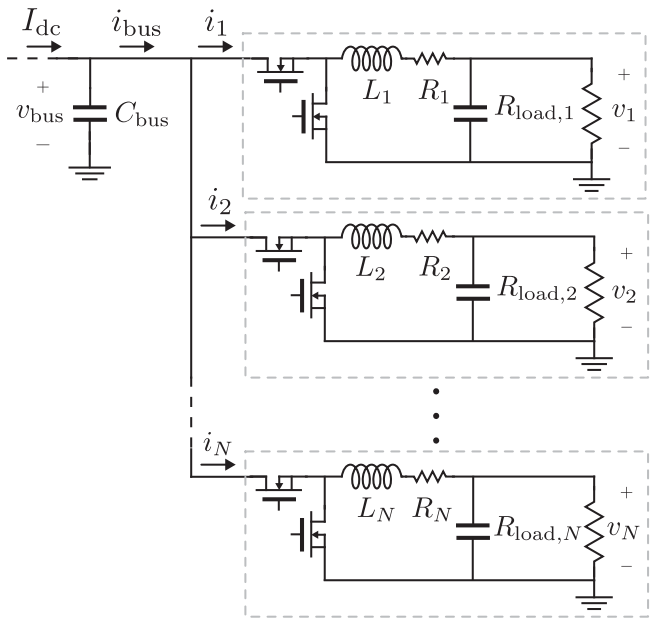

Fig. 1. System of N input-parallel connected dc–dc buck converters with independent output voltages $v_1, \ldots, v_N$ and loads modeled as resistances $R_{\rm load,1}, \ldots, R_{\rm load,N}$.

Following this mathematical definition, we will present numerical simulations that demonstrate the achievable reductions in aggregate distortion that are possible when operating at the MDP for a candidate system with three interconnected converters. Then, we will present a Monte Carlo numerical simulation that illustrates how the achievable reductions in aggregate distortion scale with the number of interconnected power converters.

A. Definition and Interpretation of Distortion

We define *distortion*, $\mathcal{D}$, as any ℓ_p-norm of the ac harmonics of a particular signal of interest. While the generality of this definition can be useful for different applications, it is perhaps most intuitive to first consider the specific scenario when $\mathcal{D}$ is defined as the squared ℓ_2-norm of the ac harmonics of $v_{\rm bus}$ in Fig. 1. With the selection of this norm, $\mathcal{D}$ is equivalent to the total harmonic distortion (or similarly the squared root mean square voltage) of $v_{\rm bus}$. In this way, $\mathcal{D}$ can be interpreted as a metric that quantifies the ac (ripple) power associated with this voltage. The minimization of this quantity is desirable in that it is proportional to the ac power handled by the capacitor(s) $C_{\rm bus}$ (which models the aggregate paralleled input capacitance of many dc–dc buck converters), and thus, dictates the volumetric size of the components as well as the losses associated with handling the ac power. While the squared ℓ_2-norm is explored in depth for this article, in other applications, the minimization of other ℓ_p-norms may

be more relevant. For instance, in integrated circuit applications, operating below the maximum voltage ratings of devices at all times is a key consideration, and thus, the minimization of the ℓ_∞-norm could be more pertinent.

B. Definition and Interpretation of the MDP

The MDP refers to the operating point of a collection of interconnected switching power converters where the distortion, $\mathcal{D}$, is minimized. In the derivation that follows, we will develop an analytic closed-form unconstrained optimization problem that explicitly defines the MDP.

For a system of N dc–dc converters, collect the relative phase spacing between converters in the length $N-1$ vector $\theta := [\theta_{21}, \theta_{32}, \ldots, \theta_{N(N-1)}]^{\mathrm{T}}$, with θ_{jk} denoting the phase spacing between the switching waveforms of the jth and kth converters, respectively. Furthermore, denote $\widetilde{v}_{\mathrm{bus}}$ as the ac voltage across C_{bus}, and $\mathcal{D}$ to be the corresponding distortion. The MDP is characterized by the θ that minimizes an unconstrained optimization problem whose cost function is the quantity $\mathcal{D}$. Precisely, the MDP corresponds to the following phase spacing:

$$\theta^\star = \arg\min_{\theta} \mathcal{D}. \tag{1}$$

The explicit parametric dependence of $\mathcal{D}$ on θ can be obtained by calculating the squared ℓ_2-norm of the Fourier coefficients of $\widetilde{v}_{\mathrm{bus}}$. From Parseval's theorem, it is also possible to determine $\mathcal{D}$ from a function norm of the time domain bus voltage waveform; that is, the squared $\mathcal{L}_2$-norm of $\widetilde{v}_{\mathrm{bus}}(t)$ [18]. However, this would not allow us to, in general, uncover the parametric dependence on θ in an analytical fashion. For the particular example of the input-parallel connected buck converters illustrated in Fig. 1, the Fourier coefficients can be obtained by computing the Fourier series of each input current, i_ℓ, $\forall \ell = 1, \ldots, N$, taking the sum of these series to obtain the corresponding series for i_{bus} and then scaling by the capacitive impedance $1/(\mathrm{j}\omega C_{\mathrm{bus}})$. Following this, it emerges that the closed-form analytical expression for $\mathcal{D}$ is

$$\mathcal{D} = \sum_{k=1}^{K}\sum_{n=1}^{N}(\beta_n^k)^2 + 4\sum_{k=1}^{K}\sum_{j=1}^{N}\sum_{i=1}^{j-1}\beta_i^k\beta_j^k\cos\left(\theta_{ij}\right) \tag{2}$$

where β_ℓ^k is a scaled version of the kth Fourier-series coefficient of i_ℓ, α_ℓ^k. The precise definitions of α_ℓ^k and β_ℓ^k as well as the complete derivation of the above expression are given in Appendix A.

With these mathematical preliminaries and definitions in place, we next provide two motivating numerical examples where we quantify the achievable improvement in power quality when operating at the MDP. Here, and in the experimental results that follow in Section III, we will use the symmetric interleaved state as a baseline for comparison. The symmetric interleaved state is equivalent to operating at the MDP when the circuit is balanced and symmetric, and thus, serves as a good baseline even in the general case for asymmetric systems.

Example 1 (Numerical analysis of the MDP with a network of three converters): Consider the $N = 3$ converter topology in Fig. 1 with component parameters and operating conditions provided in Table I. The system is intentionally operated to induce asymmetry with different output voltages, v_1, v_2, and v_3, since the resistive loads (2.4 Ω) and component parameters in each phase are otherwise identical. We perform two different sets of numerical simulations. First, we fix $v_1 = 24$ V, sweep both v_2 and v_3 independently from 12 to 36 V, and record the difference in $\mathcal{D}$ between the symmetric interleaved state and the MDP. The results of this sweep are shown in Fig. 2. (Since $\mathcal{D}$ is essentially a metric of signal power, it is natural to express reductions or changes in $\mathcal{D}$ on a decibel scale.) We observe that at certain operating points, the reduction in $\mathcal{D}$ exceeds -16 dB. This reduction is promising in that it can facilitate improvements in power quality and the minimization of components needed for filtering or EMI compliance. Moreover, $\mathcal{D}$ is lower at the MDP across every operating point in this sweep. Also, note that at the point of symmetry, $v_1 = v_2 = v_3 = 24$ V, symmetric interleaving is equivalent to operating at the MDP. Next, we perform a sweep in which v_1 is held constant at 24 V while v_2 and v_3 are swept, such that $v_3 = (48 - v_2)$ V. The results of this sweep are shown in Fig. 3, where $\mathcal{D}$ is normalized to the value obtained when $v_1 = v_2 = v_3 = 24$ V (recall that the symmetric interleaved state and the MDP are identical at this point). Across this range, the worst case $\mathcal{D}$ at the MDP is -11.28 dB lower than the value at the symmetric interleaved state, which corresponds to a 3.6× reduction in the output voltage ripple in v_{bus}.

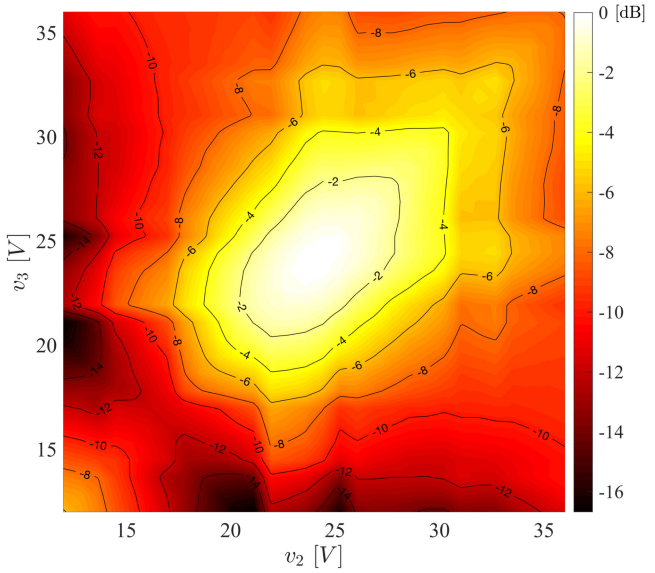

Fig. 2. Achievable reduction in $\mathcal{D}$ (in dB) when operating at the MDP compared to operating at the symmetric interleaved state. Plot shows reduction in $\mathcal{D}$ when $v_1 = 24$ V, and v_2 and v_3 are independently swept from 12 to 36 V with identical fixed resistive loads on the output of each converter. The darker areas indicate regions where greater reductions in $\mathcal{D}$ are possible.

Example 2 (Numerical analysis of the MDP for a network of N converters): In this example, we will analyze performance enhancements for arbitrarily large collections of converters with a Monte Carlo simulation. For each network of N converters (Fig. 1), one hundred scenarios with the following randomized inputs are considered: a) the output voltage v_ℓ, b) the average output current, and c) the inductor size L_ℓ of each of the N converters. The ℓth converter has an input current waveform that is pictorially represented in Fig. 13. We assume operation

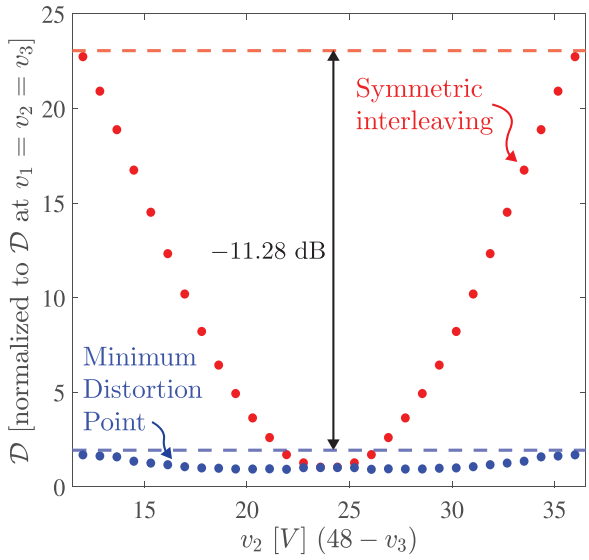

Fig. 3. Reduction in $\mathcal{D}$ between the symmetric interleaved state and the MDP when $v_1 = 24$ V and $v_3 = (48 - v_2)$ V.

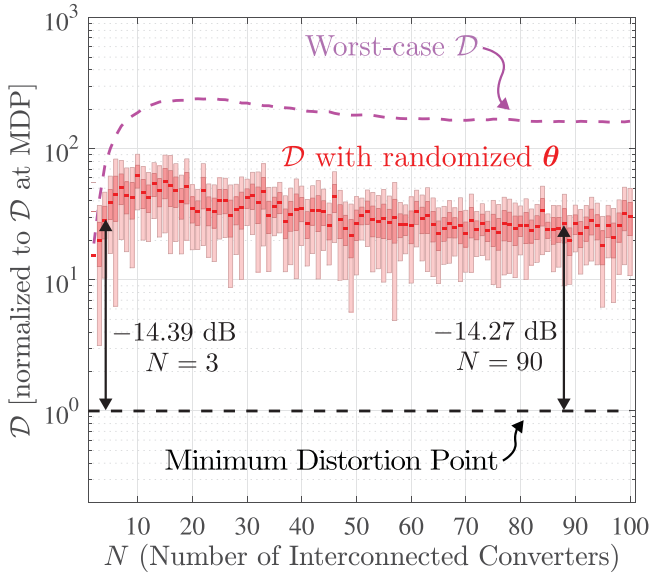

Fig. 4. Monte Carlo simulation that illustrates $\mathcal{D}$ obtained at various phase shifting scenarios, including the MDP (dashed black line), the worst-case phase shifting (dashed magenta line), and at a uniformly distributed random phase spacing across the N converters (red box plot indicating median, 25th percentile, and 75th percentile). For each N, one hundred Monte Carlo scenarios are simulated, and the output voltages, the average output current, and the inductor size of each of the N converters are randomized variables.

in periodic steady state and that the bus voltage v_{bus} and the output voltage of each converter v_ℓ are constant. Parameters are normalized for convenience (i.e., $T = 1$ and $I_\ell = 1$ p.u. nominally). For each scenario, the randomized inputs are generated as follows.

1) The duty cycle D_ℓ is a uniformly distributed random number in the interval (0.2, 0.8). Given the assumptions made, the selection of D_ℓ will determine the output voltage, v_ℓ.
2) The ripple magnitude ΔI_ℓ is a uniformly distributed random number in the interval (0.5, 1.5). The selection of ΔI_ℓ can be interpreted as the relative size of the inductance L_ℓ; i.e., a larger ΔI_ℓ corresponds to a smaller L_ℓ, and vice versa.
3) The dc output current I_ℓ is a uniformly distributed random number in the interval $(0.5, 1.5)$. The selection of I_ℓ is interpreted as the average load on the output of the ℓth converter.

For each scenario, $\mathcal{D}$ is calculated at: 1) the MDP, 2) a uniformly distributed random phase spacing across the N converters, and 3) the phase spacing across the N converters that maximizes $\mathcal{D}$, i.e., the worst-case $\mathcal{D}$ that is possible. The results of the Monte Carlo simulation are shown in Fig. 4. The data is normalized to the value of $\mathcal{D}$ at the MDP. The magenta dashed line indicates $\mathcal{D}$ obtained at the worst-case phase shifting; $\mathcal{D}$ obtained at the uniformly distributed random phase spacing across the N converters is depicted with a box plot that presents the median, the 25th percentile, and the 75th percentile of the Monte Carlo simulation.

When compared with operation at the worst-case phase shifting, operation at the MDP enables a -15.85 dB reduction in $\mathcal{D}$ when $N = 3$ and an approximately two orders of magnitude (22 dB) reduction when $N > 10$. Since it is unlikely that an uncoordinated network of power converters would ever be operated at this worst-case phase shifting, it is appropriate to also consider a comparison with $\mathcal{D}$ obtained at the uniformly distributed random phase spacing, which represents a more realistic case. Note that for this particular analysis, the symmetric interleaved state is not considered since its interpretation and implementation become impractical for larger networks of converters. Compared with operation at a randomized phase spacing, when $N = 3$, the achievable reduction in $\mathcal{D}$ is -14.39 dB from the median value, which approximately corroborates the analysis from Example 1 (Fig. 2). Furthermore, this reduction in $\mathcal{D}$ remains relatively unchanged as $N \to 100$. This analysis suggests that both small and large networks of interconnected power converters can significantly benefit from operating at the MDP, potentially achieving upwards of an order of magnitude reduction in distortion power.

III. Minimum Distortion Point Tracking (MDPT)

With the MDP formally introduced and characterized in Section II, we now present the notion of MDPT. Conceptually, we think of MDPT as control and optimization techniques synthesized to drive a system toward the MDP; that is, to uncover the optimal phase spacing given by (1). Since the unconstrained optimization problem referenced in (1) is nonconvex and of the nondeterministic polynomial time (NP) class, it does not admit an analytical solution even for the elemental case with $N = 2$. In this section, we put forth three optimization algorithms and experimentally validate their performance for the task of MDPT in dc–dc buck converters.

A. Overview of Algorithms for MDPT

The first algorithm we investigate for MDPT is based on the gradient descent method (Section IV). We will see that this method is conceptually simple and easy to implement, but relies

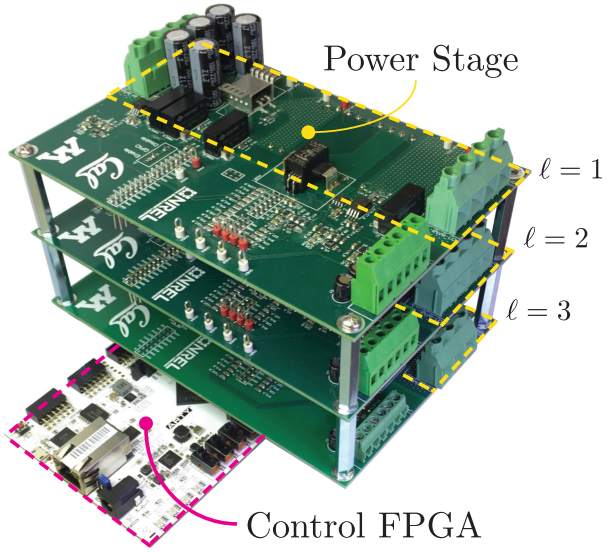

Fig. 5. Hardware prototype consisting of three 600 W input-parallel connected dc–dc buck converters with a 48 V dc input bus.

on universal and real-time knowledge of network parameters, has moderate convergence speed, and can only guarantee convergence to local minima (which may not necessarily correspond to the MDP). Second, we present an MDPT algorithm based on the NL–GS method (Section V). It will be shown that this algorithm can be completely decentralized, that is, the controller can be implemented locally for each dc–dc buck converter and does not require global knowledge of parameters, or any form of communication between converters. The tradeoff, however, is that the algorithm is more computationally intensive than the gradient method. Furthermore, only local convergence can be guaranteed. Third, we will present an MDPT algorithm based on a metaheuristic optimizer, in particular, the particle swarm optimization (PSO) computational method (Section VI). We will see that this method enables the closest convergence to the minimum (the MDP), but relies on universal real-time knowledge of the entire network and is the most computationally intensive of all three algorithms. As alluded to, each of the three presented algorithms has associated advantages and disadvantages, and these are discussed in detail and compared in Section VII. Additionally, we will discuss how local minima of the objective function will affect the steady-state performance of algorithms that can only track such minima.

B. Experimental Prototype

A hardware prototype consisting of three input-parallel connected dc–dc buck converters is used to experimentally validate the three MDPT algorithms introduced above (see Fig. 5). Each converter is rated for 600 W resulting in an overall power handling capability of 1.8 kW. Table I lists values of pertinent parameters and components of the hardware prototype. Each ℓth buck converter can locally sample the bus voltage v_{bus}, its output voltage v_ℓ, and its average output current. The bus capacitance C_{bus} is chosen to yield a bus voltage ripple ratio of approximately 6% under worst-case operating conditions. Note that this ripple ratio can be smaller, but is made intentionally large in these experiments to clearly illustrate the voltage ripple waveform. For algorithms that require a controller for each buck converter (Section V), three separate field-programmable gate array (FPGA) controller boards are used. For algorithms that require a centralized controller (Sections IV and VI), a single FPGA controller board is used (as depicted in Fig. 5).

TABLE I
PARAMETERS AND COMPONENTS FOR NUMERICAL SIMULATIONS AND EXPERIMENTAL PROTOTYPE

Parameters/Component	Value
v_{bus} (nominal)	48 V
C_{bus}	300 µF
L_ℓ	141.6 µH
R_ℓ	13.7 mΩ
Switching frequency	20 kHz
Control FPGA	Xilinx Artix-7 XC7A35T
Voltage sensor	Broadcom ACPL-C78A

Algorithm 1: Gradient Method-Based MDPT Algorithm.

1: Input: $v_{\text{bus}}, v_1 \dots v_N, I_1 \dots I_N, D_1 \dots D_N, C_{\text{bus}}$
2: Output: Steady-state minimum of (2).
3: **repeat**
4: Calculate $\mathcal{D}$ from (2)
5: Calculate gradient $\nabla\mathcal{D}(\theta[q])$
6: Calculate gradient step $\theta[q+1]$ from (3)
7: **until** stopping criterion is met

IV. MDPT Algorithm #1: Gradient Descent

A. Algorithm Principles and Design

The gradient-descent-based MDPT algorithm uses the gradient of distortion, $\mathcal{D}$, to determine a direction and magnitude in which to iteratively perturb θ toward a local minima [19]. Precisely, the update rule for the $q+1$ iterate of θ is given by

$$\theta[q+1] = \theta[q] - \kappa\nabla\mathcal{D}(\theta[q]) \tag{3}$$

where $\nabla\mathcal{D}(\theta[q])$ is the gradient of $\mathcal{D}$ with respect to θ at the qth update instant, and κ is a scalar that can be empirically determined to trade off numerical stability and convergence speed. Since $\mathcal{D}$ is not a convex function of θ, the gradient descent-based MDPT can at most converge to a local minimum depending on initial conditions. Analysis of these minima are presented in Section VII-D.

Next, we perform a numerical simulation to verify the operation of the gradient descent-based MDPT. Again, consider the topology in Fig. 1 for $N = 3$ and with the component parameters and operating conditions as indicated in Table I. We consider a static operating scenario in which $v_1 = 36$ V, $v_2 = 24$ V, and $v_3 = 12$ V. The converters are initialized to operate at the symmetric interleaved state (i.e., $\theta_{21} = 120°$ and $\theta_{31} = 240°$). We use the gradient update function in (3) to perturb θ iteratively from the symmetric interleaved initial condition. Figure 6 shows the results of the numerical simulation, i.e., θ is perturbed

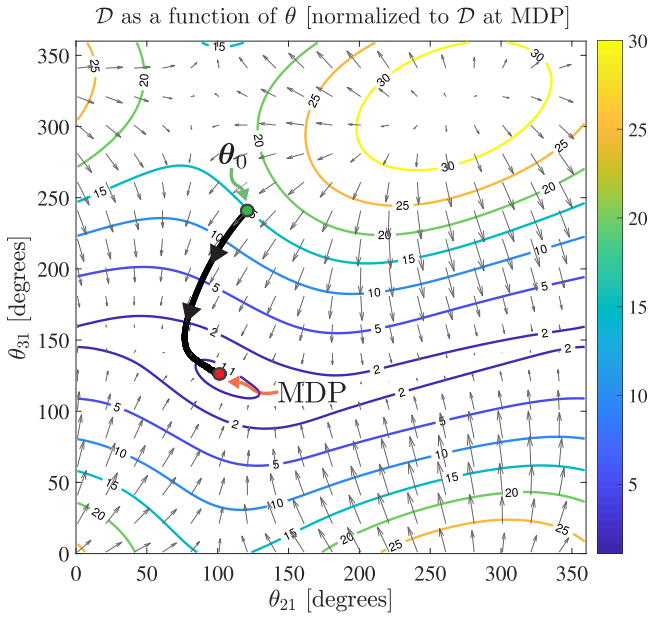

Fig. 6. Numerical simulation of the gradient-descent-based MDPT algorithm. Contour lines of $\mathcal{D}$ (normalized to $\mathcal{D}$ at the MDP) and arrows depicting $\nabla\mathcal{D}$ are shown.

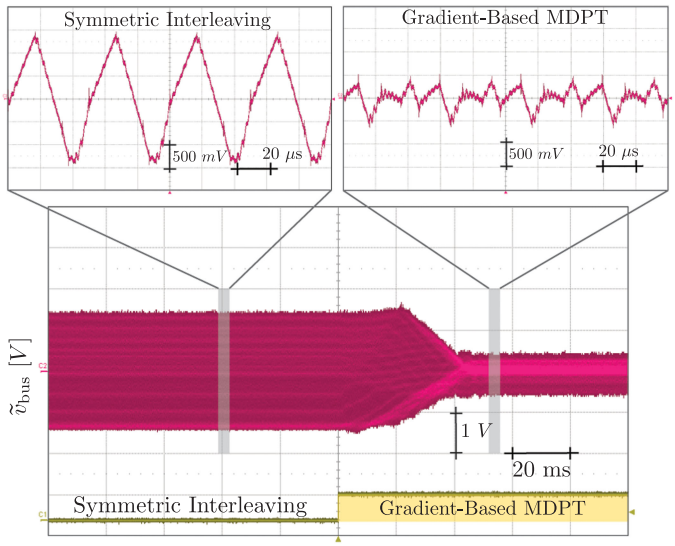

Fig. 7. Experimental validation of the convergence speed and performance of the gradient-based MDPT algorithm. As shown, the algorithm converges in approximately 100 iterations (40 ms) and enables a 2.91× reduction in the peak-to-peak ripple of $\widetilde{v}_{\text{bus}}$ compared to the symmetric interleaved state.

orthogonally to the contour lines of $\mathcal{D}$ and the algorithm converges to the MDP, in this case, at $\theta_{21} = 103°$ and $\theta_{31} = 123°$. For the particular system, $\mathcal{D}$ is reduced by -11.6 dB (14.6×) at the MDP compared to operation at the symmetric interleaved state.

B. Experimental Verification

The gradient-based MDPT algorithm is implemented on the experimental setup shown in Fig. 5. We introduced asymmetry in the resistive loads of each converter ($R_{\text{load},1} = 2.4\,\Omega$, $R_{\text{load},2} = 1.2\,\Omega$, and $R_{\text{load},3} = 1.2\,\Omega$) and also in the output voltages of each converter ($v_1 = 36$ V, $v_2 = 24$ V, and $v_3 = 12$ V).

In the first test scenario, the system is initialized at the symmetric interleaved state, and the MDPT algorithm is initiated at $t = 0$. We record the ac ripple component of v_{bus}, denoted $\widetilde{v}_{\text{bus}}$, and also the time required for the system to reach steady state. The algorithm operates at an update rate of 2.5 KHz, eight times slower than the switching frequency of each converter. This update rate can be chosen to balance convergence speed and stability of the algorithm. The precise update rate will depend on the application and the types of expected operating transients, and can be tuned in order to optimize performance. As shown in Fig. 7, when the algorithm is initialized $t = 0$, the magnitude of $\widetilde{v}_{\text{bus}}$ begins decreasing, and after about 40 ms (100 gradient iterations), the system is at steady state. At this point, the peak-to-peak ripple of $\widetilde{v}_{\text{bus}}$ is reduced 2.91× compared to the peak-to-peak ripple at the symmetric interleaved state.

Second, we validated the tracking capability of the MDPT algorithm in scenarios when the converter output loads (and thus, the MDP) are changing with respect to time. In this experiment, the output load of each converter is independently varied by changing the commanded output voltage across a fixed resistive load ($R_{\text{load},1} = R_{\text{load},2} = R_{\text{load},3} = 2.4\,\Omega$). The output voltages of the converters are initialized identically, such that $v_1 = v_2 = v_3 = 24$ V. Then, v_2 is changed linearly from 24 to 36 V at a rate of 24 V/s, while v_3 is changed linearly from 24 to 12 V at the same rate. The voltage v_1 is held constant at 24 V. Thus, the output power of two converters is dynamically varied between 60 and 540 W, while the third converter has a constant output power of 240 W.

As shown in Fig. 8(a), when symmetric interleaving is applied to this scenario, the voltage ripple in v_{bus} is minimized when the output voltages and loads are identical, as expected. However, when the asymmetries in the converter outputs are introduced, the voltage ripple increases monotonically, and reaches a maximum when $v_2 = 36$ V and $v_3 = 12$ V. At this point, the peak-to-peak ripple of $\widetilde{v}_{\text{bus}}$ is 3.28× larger than when the output voltages are identical.

When the MDPT algorithm is applied to this scenario, as shown in Fig. 8(b), the peak-to-peak ripple of $\widetilde{v}_{\text{bus}}$ stays relatively constant, even as the asymmetries in the outputs are introduced. At the point when $v_2 = 36$ V and $v_3 = 12$ V, the peak-to-peak ripple of $\widetilde{v}_{\text{bus}}$ is only 1.48× larger than when the output voltages are identical. This translates to a 2.20× reduction in the peak-to-peak ripple.

V. MDPT Algorithm #2: Decentralized Nonlinear Gauss–Seidel

A. Algorithm Principles and Design

A limitation of the gradient-based MDPT algorithm is the need for information from all N converters, including output voltages, duty cycles, and average output currents. In some applications, it is desirable to have a local controller at each

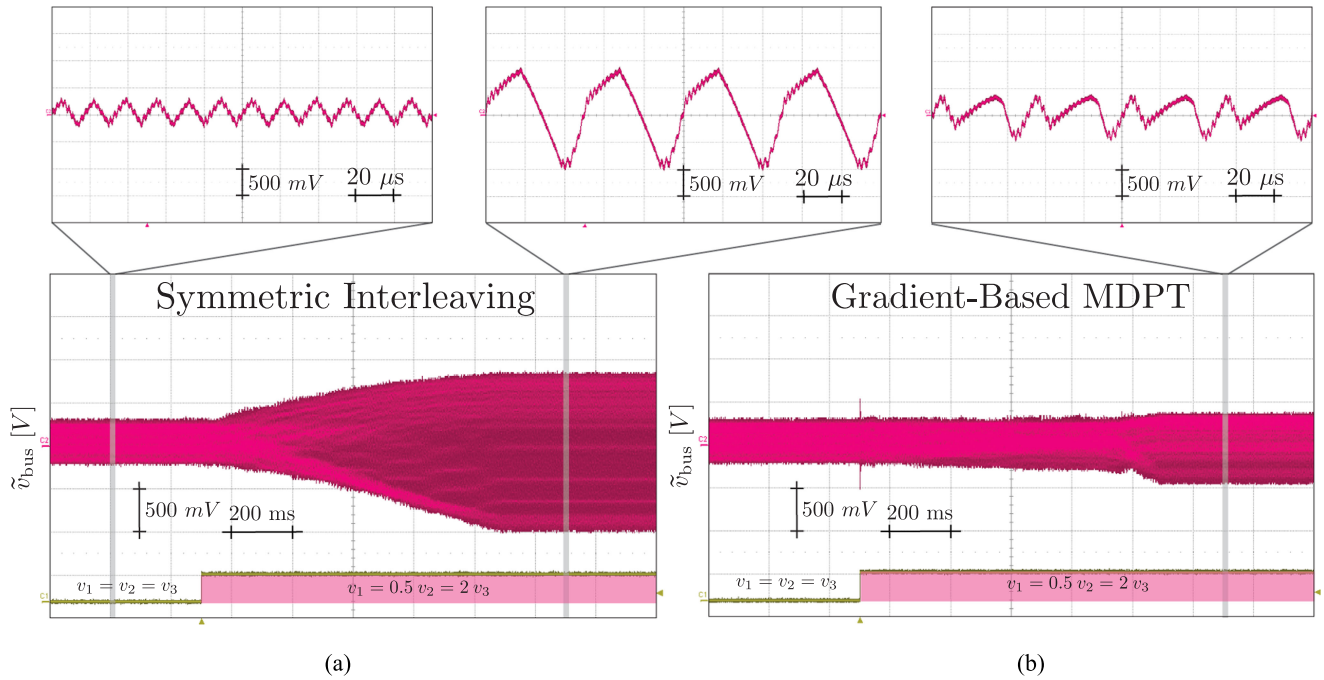

Fig. 8. Experimental validation of the tracking capability of the gradient-based MDPT algorithm for time-varying loads. As asymmetries in the output loads are gradually introduced at $t = 500$ ms, (a) symmetric interleaving results in a 3.28× larger peak-to-peak ripple of $\widetilde{v}_{\rm bus}$ at the worst case, while (b) the gradient-based MDPT algorithm enables ripple minimization throughout the asymmetric loading transient and results in only 1.48× larger peak-to-peak ripple of $\widetilde{v}_{\rm bus}$ at the worst case.

Algorithm 2: Decentralized NL–GS-Based MDPT Algorithm.

1: Output: Steady state minimum of (2).
2: **for** $\ell = 1$ to N **do**
3: Input: $v_{\rm bus}, v_\ell, I_\ell, D_\ell, C_{\rm bus}$
4: Output: Phase spacing $\theta_\ell^\star$ corresponding to the minimizer of $\mathcal{D}$
5: **repeat**
6: Assume constant θ vector except for θ_ℓ component
7: Calculate $\mathcal{D}$ from inputs
8: Computation of $\theta_\ell^\star$ that minimizes $\mathcal{D}$
9: **until** stopping criterion is met

power converter that only samples and utilizes local information. Such a decentralized operating paradigm has obvious benefits with regard to modularity, scalability, and fault tolerance.

Here, we present an MDPT algorithm based on a decentralized NL–GS technique. Conceptually, the NL–GS MDPT algorithm minimizes (2) one "component" at a time, where a component is the phase shift θ_ℓ of a single converter. For the ℓth converter, we calculate the $\theta_\ell^\star$ that globally minimizes $\mathcal{D}$ under the assumption that all other components of the vector θ are constant. Because this is a one-dimensional optimization problem, it is simple to compute, and the global minimum can be obtained using a brute-force method. Note that this minimum is different from the MDP since it constrains the other $N-1$ components of θ. By successively calculating $\theta_\ell^\star$ for all N converters and iterating the calculations, it can be proven that this successive component-wise minimization will yield convergence to a *local* minima of $\mathcal{D}$ [20]. These local minima will be identical to the minima obtained by the gradient-based MDPT algorithm.

The local minimization of each component only requires information that can be sampled by the ℓth converter, namely $v_{\rm bus}, v_\ell, I_\ell, D_\ell$, and $C_{\rm bus}$. In this way, the algorithm can be implemented locally at each converter and requires no communication with any other controller. We assume that each converter calculates and updates its $\theta_\ell^\star$ asynchronously, which enables us to make the needed assumption that every phase shift other than θ_ℓ is constant. The experimental results that follow validate the practicality of this assumption.

Next, we perform a numerical Monte Carlo simulation to verify the operation and convergence of the NL–GS MDPT algorithm. The setup details of the Monte Carlo simulation are identical to those shown previously in Example 2 and Section VII-D. Fig. 9 illustrates the value of $\mathcal{D}$ obtained after q iterations of the NL–GS MDPT algorithm for $N = 3$, 20, and 100. In each iteration q, the N converters each compute the optimizer $\theta_\ell^\star$ once.

The results of the simulation demonstrate that the NL–GS MDPT algorithm indeed asymptotically converges toward the local minima identified in Section VII-D. Moreover, as our previous analysis indicated, the local minima of larger networks (e.g., $N = 100$) are closer to the MDP and can yield better steady-state solutions. The convergence rate of the NL–GS MDPT algorithm also has a dependence on the size of the network. Smaller networks have longer convergence times to steady state, and also have larger variance in the value of $\mathcal{D}$. This can be seen with the shaded regions in Fig. 9, which indicate the 25th and 75th

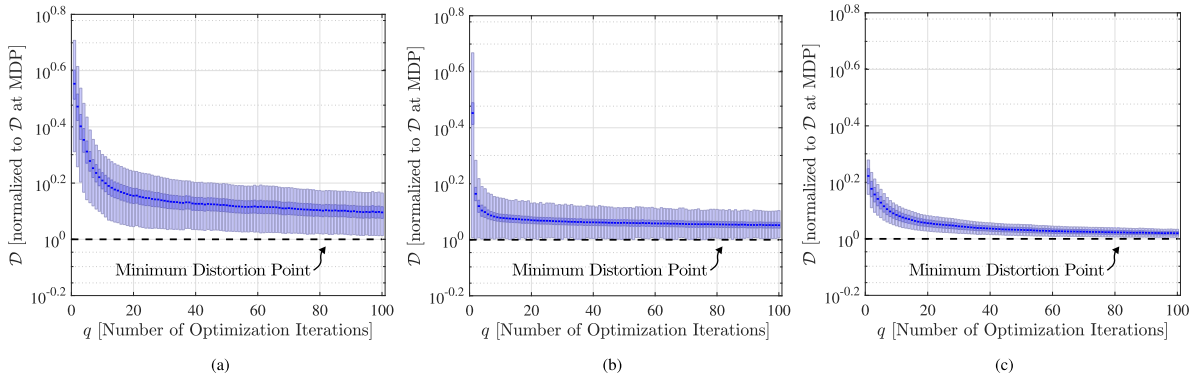

Fig. 9. Monte Carlo simulation that illustrates the value of $\mathcal{D}$, normalized to $\mathcal{D}$ at the MDP, obtained for q iterations of the NL–GS MDPT algorithm. As shown, the NL–GS MDPT algorithm converges asymptotically towards local minima identified in Section VII-D, while increasing the number of interconnected converters (N) yields a steady-state solution closer to the MDP. (a) $N = 3$. (b) $N = 20$. (c) $N = 100$.

percentile values of the Monte Carlo simulation. For networks of most sizes, the analysis suggests that the NL–GS MDPT algorithm will obtain an adequate solution in approximately fifty iterations.

B. Experimental Verification

We implemented the NL–GS MDPT algorithm on the experimental setup shown in Fig. 5. The setup is modified, such that each dc–dc buck converter has a separate FPGA controller that runs Algorithm 2. The same circuit and asymmetric operating parameters from the first test in Section IV-B are used, that is, $R_{\text{load},1} = 2.4\,\Omega$, $R_{\text{load},2} = 1.2\,\Omega$, and $R_{\text{load},3} = 1.2\,\Omega$ and $v_1 = 36\,\text{V}$, $v_2 = 24\,\text{V}$, and $v_3 = 12\,\text{V}$. Each converter calculates and updates its corresponding θ_ℓ at a rate of 2.5 kHz. The clocks of the controllers are not synchronized with each other, and successive θ_ℓ updates are considered asynchronous due to inherent clock drift.

Again, the system is initialized at the symmetric interleaved state, and the NL–GS MDPT algorithm is initiated at $t = 0$. We present the ac ripple component $\widetilde{v}_{\text{bus}}$ in Fig. 10. When the algorithm is initialized at time $t = 0$, the peak-to-peak ripple magnitude of $\widetilde{v}_{\text{bus}}$ begins decreasing. After about 30 ms (75 component-wise iterations), the system is at steady state. At this point, the peak-to-peak ripple of $\widetilde{v}_{\text{bus}}$ is reduced 2.82× compared to the peak-to-peak ripple at the symmetric interleaved state.

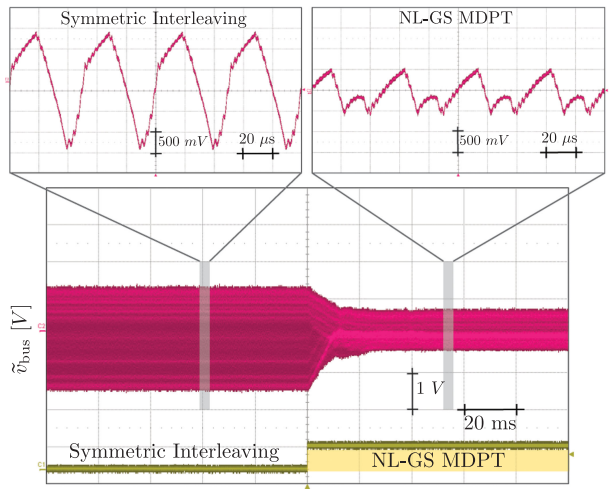

Fig. 10. Experimental validation of the convergence speed and performance of the decentralized NL–GS-based MDPT algorithm. As shown, the algorithm converges in approximately 75 component-wise iterations (30 ms) and enables a 2.82× reduction in the peak-to-peak ripple of $\widetilde{v}_{\text{bus}}$ compared to the peak-to-peak ripple at the symmetric interleaved state.

VI. MDPT Algorithm #3: Metaheuristic Optimizer

A. Algorithm Principles and Design

Metaheuristic optimization techniques are generally empirical in nature and do not have theoretical guarantees of convergence or optimality. However, in optimization problems with large feasible solution spaces, metaheuristics can, in some cases, find reasonably good solutions with less computational effort than a brute force search. We explore the application of metaheuristics for the MDPT problem by implementing a metaheuristic technique, specifically, the particle swarm optimization (PSO) method [21], [22].

Algorithm 3: Metaheuristic Optimizer (Particle Swarm Optimizer) MDPT Algorithm.

1: Input: $v_{\text{bus}}, v_1 \ldots v_N, I_1 \ldots I_N, D_1 \ldots D_N, C_{\text{bus}}$
2: Output: Steady state minimum of (2).
3: Generate $\mathcal{I}$ particles of θ, θ^i, that are initialized at uniformly distributed random points within the domain $\theta_\ell \in [0, 2\pi)$
4: Associate velocity V^i, personal best p^i, velocity update rule $\mu^i(\theta^i, V^i)$, and position update rule $\xi^i(\theta^i, V^i)$ vectors with every i^{th} particle
5: **repeat**
6: **for** $i = 1$ to $\mathcal{I}$ **do**
7: Calculate $\mathcal{D}(\theta^i)$ from (2)
8: **if** $\mathcal{D} < \min(p^i)$ **then**
9: Update p^i with $\mathcal{D}$
10: Update θ^i from $\xi^i(\theta^i, V^i)$
11: Update V^i from $\mu^i(\theta^i, V^i)$
12: **until** stopping criterion is met

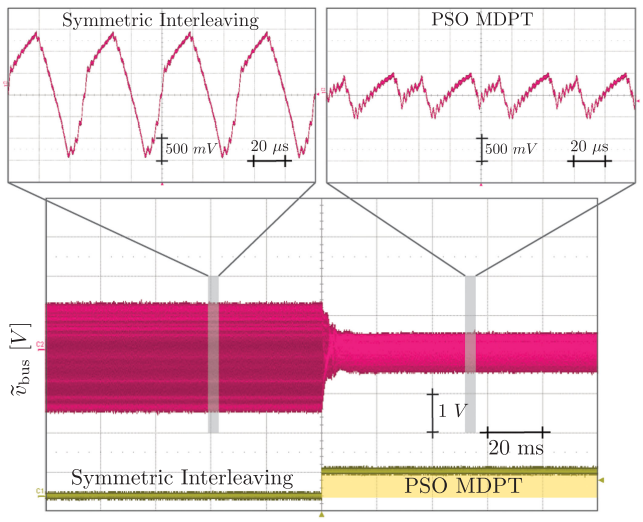

Fig. 11. Experimental validation of the convergence speed and performance of the metaheuristic optimizer-based MDPT algorithm. As shown, the algorithm converges in approximately 12 iterations (5 ms) and enables a 3.06× reduction in the peak-to-peak ripple of $\widetilde{v}_{\rm bus}$ compared to the peak-to-peak ripple at the symmetric interleaved state.

A sketch of the PSO MDPT algorithm is presented in Algorithm 3. As shown, the algorithm generates $\mathcal{I}$ "particles," or instances, of θ, denoted as θ^i, that are initialized with a uniform random distribution. The distortion $\mathcal{D}$ is calculated at each of the $\mathcal{I}$ particles from (2). Similar to the gradient-based MDPT algorithm, this requires information from all N converters, including output voltages, duty cycles, and average output currents. Thus, unlike the NL–GS MDPT algorithm, it is not a decentralized technique. Once $\mathcal{D}$ is calculated, each particle stores the lowest $\mathcal{D}$ it has computed thus far in a "personal best" vector p^i. New values for θ^i are then calculated based on "velocity" and "position" update rules, $\mu^i(\theta^i, V^i)$ and $\xi^i(\theta^i, V^i)$, respectively. The PSO MDPT can be computationally intensive since the number of evaluations of $\mathcal{D}$ scale linearly with the number of particles $\mathcal{I}$. However, increasing the number of particles is generally desirable since it increases the probability of obtaining a minimum at or close to the global minimum of the objective function and avoiding suboptimal local minima.

B. Experimental Verification

We implemented the PSO MDPT algorithm on the experimental setup shown in Fig. 5 with a single FPGA controller. The same circuit and asymmetric operating parameters from the first test in Section IV-B and V-B are used, that is, $R_{\rm load,1} = 2.4\,\Omega$, $R_{\rm load,2} = 1.2\,\Omega$, and $R_{\rm load,3} = 1.2\,\Omega$ and $v_1 = 36\,\text{V}, v_2 = 24\,\text{V}$, and $v_3 = 12\,\text{V}$. The PSO algorithm is implemented with $\mathcal{I} = 128$, and updates the optimal phase spacing $\theta^\star$ at a rate of 2.5 kHz. As shown in Fig. 11, the system is initialized at the symmetric interleaved state, and the PSO MDPT algorithm is initiated at $t = 0$. Within 5 ms (12 PSO iterations), a steady-state value is reached where the peak-to-peak ripple of $\widetilde{v}_{\rm bus}$ is reduced 3.06× compared to the peak-to-peak ripple at the symmetric interleaved state.

VII. MDPT Algorithm Analysis and Tradeoffs

With three candidate algorithms for MDPT presented in Sections IV, V, and VI, we will now analyze the advantages and disadvantages of each, as well as discuss candidate application areas where a particular algorithm would be better suited than the others. The algorithms are compared based on four performance metrics: 1) computational complexity, 2) convergence speed, 3) decentralization of control, and 4) achievable degree of distortion minimization at steady state. Table II presents a summary of these comparison metrics.

A. Computational Complexity

To quantify the computational complexity of each of the algorithms, we refer to the slice lookup table (LUT) instances and slice register instances used by the algorithm on the Xilinx Artix-7 XC7A35T FPGA. The XC7A35T contains 20 800 slice LUTs and 41 600 slice registers. Of the three algorithms, the gradient-based MDPT algorithm has the lowest complexity, utilizing only 2.32% of the slice LUTs and 0.33% of the slice registers. The low computational complexity and ease of implementation make the gradient-based MDPT algorithm well-suited for applications that demand low-cost and are not physically distributed (e.g., board-level point-of-load converters). The NL–GS MDPT algorithm has slightly higher complexity; however, a key difference is that the NL–GS MDPT algorithm requires an FPGA for *each* of the N power converters. The PSO-based MDPT algorithm is by far the most computationally complex of the three algorithms, requiring 81.3% of the slice LUTs and 11.5% of the slice registers. While the PSO algorithm itself is simple to implement in principle and also practically on an FPGA, the large number of computations make the algorithm resource intensive. In particular, the number of evaluations of $\mathcal{D}$ scale linearly with the number of particles $\mathcal{I}$ to evaluate. Thus, a tradeoff between resource utilization and algorithm performance is necessary, since more particles will improve the optimality of the algorithm. Here, we conclude that for resource-constrained computational systems, the gradient-based and NL–GS MDPT algorithms are most attractive, while the PSO MDPT algorithm is better suited to high performance computational systems and networks with lower N.

B. Convergence Speed

Next, we will compare the convergence speed of each algorithm to steady state. We reference the experimental results obtained in Sections IV-B, V-B, and VI-B that verified the convergence of each algorithm when initialized from the symmetric interleaved state. The gradient-based MDPT algorithm has the slowest convergence rate, requiring 100 algorithm iterations to converge. As discussed, the scalar value κ in (3) dictates the numerical stability and convergence speed. Here, κ was selected to maximize the convergence speed while ensuring numerical stability over a wide operating range. Note that similar Newton-derived techniques, such as the secant method, may provide improvements in convergence speed and stability for

TABLE II
A QUANTITATIVE COMPARISON OF THE THREE MDPT ALGORITHMS PRESENTED IN THIS ARTICLE

	Gradient-Based MDPT	NL-GS MDPT	PSO MDPT
Computational Complexity[1,2] Slice LUT Instances/Slice Register Instances Percent Utilization of FPGA Resources	483 / 137 (2.32 % / 0.33 %)	609 / 306 (2.93 % / 0.74 %)	16905 / 4795 (81.3 % / 11.5 %)
Convergence Speed[1,3]	40 ms (100 algorithm iterations)	30 ms (75 algorithm iterations)	5 ms (12 algorithm iterations)
Decentralized?	No	Yes	No
Minima Obtained Compared to MDP[1,4]	1.2	1.2	1.0
Candidate Application Areas	point-of-load converters	dc microgrids	on-die voltage regulation modules

[1]Lower is better.
[2]For algorithm block only on Xilinx Artix-7 XC7A35 T.
[3]From experimental results in Sections IV-B, V-B, and VI-B.
[4]From median value of analysis in Section VII-D for $N = 3$; 1.0 is optimal.

gradient-type algorithms. The NL–GS MDPT algorithm provides moderate improvements in convergence speed compared to the gradient-based MDPT algorithm, but is similarly limited in performance since each calculation only perturbs a single component (i.e., one dimension of θ) at a time. The PSO MDPT algorithm has the fastest convergence speed, requiring only 12 algorithm iterations to achieve steady state. This can be attributed to the nature of the metaheuristic optimization, which does not perturb θ smoothly, but can instantaneously shift θ to a better performing point in the feasible search space.

C. Decentralization of Control

Both the gradient-based and PSO MDPT algorithms are centralized; that is, they required information from all N converters, including output voltages, duty cycles, and average output currents. While this may be practical in some applications, such as in point-of-load converters and on-die power conversion, it is unrealistic in others, such as in microgrids and building power distribution networks. The spatially distributed nature of these latter applications make it challenging to communicate information in real-time to a centralized controller. Moreover, this centralized controller introduces a single point of failure in the system. To overcome these limitations, the NL–GS MDPT algorithm offers a decentralized approach that only requires information that is local to each power converter. Thus, for applications that are inherently spatially separated or that require high degrees of scalability, modularity, or fault tolerance, the NL–GS MDPT algorithm offers compelling benefits.

D. Achievable Degree of Distortion Minimization

Finally, we analyze and compare the minima obtained by each algorithm. Since problem (2) is nonconvex, the gradient-based and NL–GS MDPT algorithm will track local minima of $\mathcal{D}(\theta)$ depending on the initial condition of θ. For instance, in Fig. 6, a second minima can be seen around $\theta_{21} = 275^\circ$ and $\theta_{31} = 325^\circ$, and if θ were initialized closer to this region, then convergence to this suboptimal minima would be likely. Thus, it is important to study if these local minima are sufficiently "good" as to justify the use of optimization algorithms that can only track such minima.

Toward this end, we performed another Monte Carlo simulation for analyzing the distortion $\mathcal{D}$ obtained at these local minima in relation to $\mathcal{D}$ obtained at the MDP. The setup details of the Monte Carlo simulation are identical to those in Example 2. A local minimum is identified through the selection of a uniformly distributed random initial condition. We run one hundred scenarios with the randomized inputs for each network of N interconnected power converters (Fig. 1). The results are shown in Fig. 12, where the magenta dashed line is $\mathcal{D}$ at the worst-case phase shifting, the data in red is $\mathcal{D}$ at the uniformly distributed random phase spacing across the N converters, and the data in blue is $\mathcal{D}$ at the randomly selected local minima. The values of $\mathcal{D}$ have been normalized to the value of $\mathcal{D}$ at the MDP and plotted on a logarithmic scale. Again, the shaded regions around each data point indicate the 25th and 75th percentiles of the Monte Carlo simulation, while the dark line represents the median value. The right subfigure illustrates a zoomed version of $\mathcal{D}$ obtained at the local minima on a linear scale in relation to $\mathcal{D}$ at the MDP.

The results indicate that for networks composed of $N < 20$ interconnected power converters, the distortion $\mathcal{D}$ obtained at local minima are generally in the range of 1 to 2.5$\times$ the distortion obtained at the MDP. This can still be considered a significant reduction, particularly in relation to $\mathcal{D}$ obtained at the worst-case phase shifting, which, for this range of network size, results in 5 to 10$\times$ higher $\mathcal{D}$ than the local minima. Interestingly, for larger networks ($N > 20$), we see that $\mathcal{D}$ obtained at local minima begin to converge to the value of $\mathcal{D}$ obtained at the MDP. Indeed, at $N = 100$, the minima are essentially identical. This can be attributed, in part, to the observation that the degrees of freedom in the optimization problem scale linearly with the number of converters in the network. Thus, as N increases, there can be more local minima that are closer to the MDP. The analysis suggests that optimization methods that track local minima can be adequate for the MDPT problem, and can be particularly effective at obtaining close-to-optimal performance when applied to larger networks.

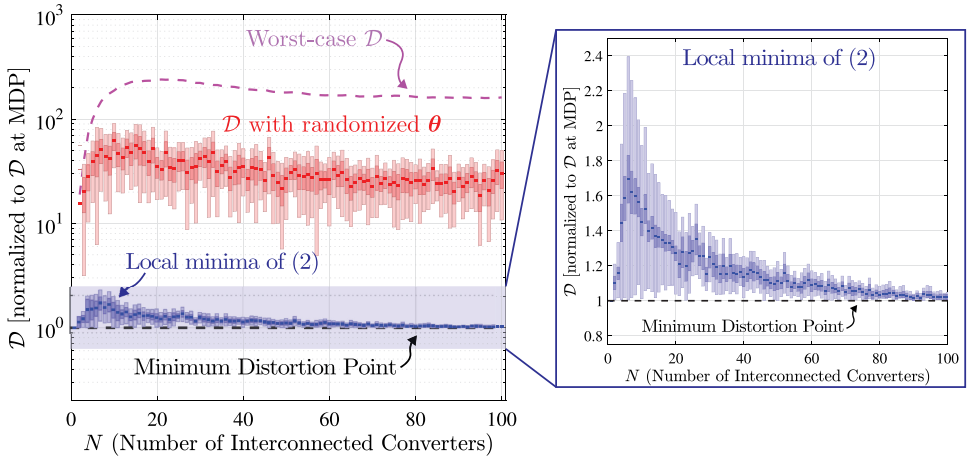

Fig. 12. Monte Carlo simulation that illustrates $\mathcal{D}$ obtained at the worst-case phase shifting (dashed magenta line), at a uniformly distributed random phase spacing across the N converters (red), and at various local minima of the non-convex function $\mathcal{D}(\theta)$ (blue), all normalized to $\mathcal{D}$ at the MDP, and plotted as a function of the number of interconnected power converters N. For each N, one hundred scenarios are simulated, and the 25th and 75th percentile values of $\mathcal{D}$ are shown with shaded bars.

Conversely, the PSO-based MDPT algorithm has a key advantage in that, due to the stochastic nature of particle position and velocity, it is significantly less likely to become trapped in local minima. Moreover, increasing the number of particles enables faster identification of solutions that are practically identical to the MDP. However, since the PSO-based MDPT algorithm (or most metaheuristic optimization techniques in general) does not have theoretical guarantees of stability or convergence to the MDP, numerical simulations should be used to verify performance and convergence under expected operating conditions. The high-performance yet high computational complexity of the PSO-based MDPT algorithm makes it well-suited for applications that are not resource-constrained, for instance, on-die voltage regulation modules.

VIII. Conclusions and Directions for Future Work

This article introduced the notion of MDPT as a means to minimize distortion in networks of series- or parallel-connected dc–dc converters. Our analysis for networks of up to 100 interconnected power converters indicated that a one to two orders of magnitude reduction (-14 to -22 dB) in distortion power is possible when operating at the MDP, resulting in reduced aggregate ripple. We presented and experimentally verified algorithms that can dynamically solve the MDPT optimization problem. The three algorithms—based on the gradient method, the NL–GS method, and a metaheuristic optimizer—each have unique properties that make them well-suited for a variety of diverse applications. Practically, MDPT can enable improvements in power quality and reductions in filter requirements (and subsequently, volume) for a broad array of use cases, including point-of-load conversion systems, dc microgrids, and power management integrated circuits. Future directions for research include considerations for ac systems, weighted cost functions, techniques for high-bandwidth distortion sensing, and algorithmic improvements to minimize the impact of steady-state oscillations and limit cycles.

Appendix A
Uncovering the Dependence of $\mathcal{D}$ on θ

Consider the topology in Fig. 1. Let $\widetilde{v}_{\rm bus}$ be the ripple (ac) voltage across $C_{\rm bus}$. We assume that $I_{\rm dc}$ contributes the dc component of $i_{\rm bus}$, while $C_{\rm bus}$ contributes the ac component of $i_{\rm bus}$. In this way, $\widetilde{v}_{\rm bus}$ is a function of the ac component of $i_{\rm bus}$. The input current to each converter i_ℓ has a real-form Fourier series

$$i_\ell(t) = \frac{a_\ell^0}{2} + \sum_{k=1}^{\infty} a_\ell^k \cos(2\pi k t) + b_\ell^k \sin(2\pi k t). \tag{4}$$

The Fourier coefficients a_ℓ^k and b_ℓ^k are given by

$$a_\ell^k = \frac{2}{D_\ell \xi_k^2}\Delta I_\ell \cos(D_\ell \xi_k) + \frac{1}{\xi_k}(\Delta I_\ell + 2I_\ell)\sin(D_\ell \xi_k) \tag{5}$$

$$b_\ell^k = \frac{2}{D_\ell \xi_k^2}\Delta I_\ell \sin(D_\ell \xi_k) + \frac{1}{\xi_k}\left(\Delta I_\ell - 2I_\ell + (\Delta I_\ell + 2I_\ell)\cos(D_\ell \xi_k)\right) \tag{6}$$

where $\xi_k = 2\pi k T$ and $\Delta I_\ell, I_\ell, D_\ell$, and T are pictorially defined in Fig. 13.

We can express (4) in complex-exponential form as

$$i_\ell(t) = \sum_{k=-\infty}^{\infty} \alpha_\ell^k e^{j2\pi k t} \tag{7}$$

where $\alpha_\ell^k := |\alpha_\ell^k| e^{j\psi_\ell^k}$, with

$$|\alpha_\ell^k| := \frac{1}{2}((a_\ell^k)^2 + (b_\ell^k)^2)^{\frac{1}{2}} \tag{8}$$

$$\psi_\ell^k := -\arctan\left(\frac{b_\ell^k}{a_\ell^k}\right). \tag{9}$$

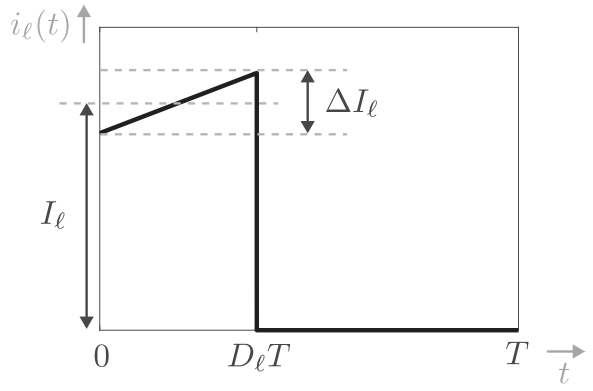

Fig. 13. Time domain sketch of one period of $i_\ell(t)$.

With this in place, let us now derive the Fourier-series coefficients of $i_{\rm bus}$ as

$$i_{\rm bus}(t) = \sum_{\ell=1}^{N} i_\ell(t) \tag{10}$$

$$= \sum_{\ell=1}^{N} \sum_{k=-\infty}^{\infty} (\alpha_\ell^k \mathrm{e}^{\mathrm{j}2\pi kt}) \mathrm{e}^{-\mathrm{j}\xi_k\theta_\ell} \tag{11}$$

where θ_ℓ is the phase shift of i_ℓ with reference to an arbitrary reference angle. Note that (10) follows from Kirchhoff's current law (KCL), while in (11), we have substituted for each i_ℓ from (7), and the factor $\mathrm{e}^{-\mathrm{j}\xi_k\theta_\ell}$ accounts for the phase shift θ_ℓ [23]. Since $i_{\rm bus}$ and $\widetilde{v}_{\rm bus}$ are linearly related by the capacitive impedance, we can obtain the Fourier series of $\widetilde{v}_{\rm bus}$ as follows:

$$\widetilde{v}_{\rm bus}(t) = \sum_{\ell=1}^{N} \sum_{k=-\infty}^{\infty} \frac{1}{\mathrm{j}2\pi kC_{\rm bus}} \alpha_\ell^k \mathrm{e}^{\mathrm{j}2\pi kt} \mathrm{e}^{-\mathrm{j}\xi_k\theta_\ell}.$$

$$=: \sum_{\ell=1}^{N} \sum_{k=-\infty}^{\infty} \beta_\ell^k \mathrm{e}^{\mathrm{j}2\pi kt} \mathrm{e}^{-\mathrm{j}\xi_k\theta_\ell}. \tag{12}$$

Applying Parseval's theorem [23] and terminating the pertinent summation to some finite $K \in \mathbb{Z}^+$, we get the expression for $\mathcal{D}$ in (2).

REFERENCES

[1] J. Poon, B. B. Johnson, S. V. Dhople, and S. R. Sanders, "Minimum distortion point tracking: Optimal phase shifting for input- or output-parallel connected dc-dc converters," in *Proc. IEEE 19th Workshop Control Modeling Power Electron.*, Jun. 2018, pp. 1–6.

[2] E. A. Burton *et al.*, "FIVR—Fully integrated voltage regulators on 4th generation Intel Core SoCs," in *Proc. IEEE Appl. Power Electron. Conf. Exp.*, Mar. 2014, pp. 432–439.

[3] P. A. Madduri, J. Poon, J. Rosa, M. Podolsky, E. A. Brewer, and S. R. Sanders, "Scalable dc microgrids for rural electrification in emerging regions," *IEEE J. Emerg. Sel. Topics Power Electron.*, vol. 4, no. 4, pp. 1195–1205, Dec. 2016.

[4] L. F. Casey and M. F. Schlecht, "A high-frequency, low volume, point-of-load power supply for distributed power systems," *IEEE Trans. Power Electron.*, vol. 3, no. 1, pp. 72–82, Jan. 1988.

[5] B. A. Miwa, D. M. Otten, and M. E. Schlecht, "High efficiency power factor correction using interleaving techniques," in *Proc. 7th Annu. Appl. Power Electron. Conf. Expo.*, Feb. 1992, pp. 557–568.

[6] C. Chang and M. A. Knights, "Interleaving technique in distributed power conversion systems," *IEEE Trans. Circuits Syst. I: Fundamental Theory Appl.*, vol. 42, no. 5, pp. 245–251, May 1995.

[7] D. J. Perreault and J. G. Kassakian, "Distributed interleaving of paralleled power converters," *IEEE Trans. Circuits Syst. I: Fundamental Theory Appl.*, vol. 44, no. 8, pp. 728–734, Aug. 1997.

[8] M. Sinha, J. Poon, B. B. Johnson, M. Rodriguez, and S. V. Dhople, "Decentralized interleaving of parallel-connected buck converters," *IEEE Trans. Power Electron.*, vol. 34, no. 5, pp. 4993–5006, May 2019.

[9] H. S. Patel and R. G. Hoft, "Generalized techniques of harmonic elimination and voltage control in thyristor inverters: Part I–harmonic elimination," *IEEE Trans. Industry Appl.*, vol. IA-9, no. 3, pp. 310–317, May 1973.

[10] I. J. Pitel, S. N. Talukdar, and P. Wood, "Characterization of programmed-waveform pulsewidth modulation," *IEEE Trans. Industry Appl.*, vol. IA-16, no. 5, pp. 707–715, Sep. 1980.

[11] J. Rodriguez, J.-S. Lai, and Z. Peng, "Multilevel inverters: A survey of topologies, controls, and applications," *IEEE Trans. Ind. Electron.*, vol. 49, no. 4, pp. 724–738, Aug. 2002.

[12] J. Kassakian, M. Schlecht, and G. Verghese, *Principles of Power Electronics*. Reading, MA, USA: Addison-Wesley, 1991.

[13] T. Beechner and J. Sun, "Asymmetric interleaving a new approach to operating parallel converters," in *Proc. IEEE Energy Convers. Congr. Expo.*, Sep. 2009, pp. 99–105.

[14] M. Schuck and R. C. N. Pilawa-Podgurski, "Ripple minimization through harmonic elimination in asymmetric interleaved multiphase dc-dc converters," *IEEE Trans. Power Electron.*, vol. 30, no. 12, pp. 7202–7214, Dec. 2015.

[15] A. C. Wang and S. R. Sanders, "Programmed pulsewidth modulated waveforms for electromagnetic interference mitigation in dc-dc converters," *IEEE Trans. Power Electron.*, vol. 8, no. 4, pp. 596–605, Oct. 1993.

[16] A. M. Stankovic, G. E. Verghese, and D. J. Perreault, "Analysis and synthesis of randomized modulation schemes for power converters," *IEEE Trans. Power Electron.*, vol. 10, no. 6, pp. 680–693, Nov. 1995.

[17] S. Banerjee and G. Verghese, *Nonlinear Phenomena in Power Electronics: Bifurcations, Chaos, Control, and Applications*. Hoboken, NJ, USA: Wiley, 2001.

[18] F. Callier and C. Desoer, *Linear System Theory*. Berlin, Germany: Springer-Verlag, 1991.

[19] S. Boyd and L. Vandenberghe, *Convex Optimization*. Cambridge, U.K.: Cambridge Univ. Press, 2004.

[20] D. P. Bertsekas and J. N. Tsitsiklis, *Parallel and Distributed Computation: Numerical Methods*. Belmont, MA, USA: Athena Scientific, 1997.

[21] J. Kennedy and R. Eberhart, "Particle swarm optimization," in *Proc. Int. Conf. Neural Netw.*, vol. 4, Nov 1995, pp. 1942–1948.

[22] J. Kennedy and R. C. Eberhart, *Swarm Intelligence*. San Mateo, CA, USA: Morgan Kaufmann, 2001.

[23] A. V. Oppenheim, A. S. Willsky, and S. H. Nawab, *Signals and Systems*, 2nd ed. Upper Saddle River, NJ, USA: Prentice-Hall, 1996.

Jason Poon (Member, IEEE) received the B.S. degree from the Olin College of Engineering, Needham, MA, USA, in 2012, and the M.S. and Ph.D. degrees from the University of California, Berkeley, CA, USA, in 2015 and 2019, all in electrical engineering.

He is currently a Postdoctoral Scholar with the Department of Electrical Engineering at Stanford University, Stanford, CA, USA, and also, an Affiliate Researcher with the Lawrence Berkeley National Laboratory, Berkeley, CA, USA. He has held various R&D positions at Dialog Semiconductor, ABB Corporate Research, NREL, MIT, the National University of Singapore, and Typhoon HIL. His research interests include power electronics and renewable energy systems.

Dr. Poon is the recipient of the 2019 EERE Postdoctoral Research Award and the Best Paper Award at the 2016 IEEE Workshop on Control and Modeling for Power Electronics for his work on distributed fault-tolerant power electronics.

Brian Johnson (Member, IEEE) received the M.S. and Ph.D. degrees in electrical and computer engineering from the University of Illinois at Urbana-Champaign, Urbana, IL, USA, in 2010 and 2013, respectively.

He is the Washington Research Foundation Innovation Assistant Professor with the Department of Electrical and Computer Engineering at the University of Washington, Forks Ave, Forks, WA, USA. Prior to joining the University of Washington in 2018, he was an Engineer with the National Renewable Energy Laboratory in Golden, CO, USA. His research interests include renewable energy systems, power electronics, and control systems.

Dr. Johnson currently serves as an Associate Editor for the IEEE TRANSACTIONS ON ENERGY CONVERSION.

Sairaj V. Dhople (Member, IEEE) received the B.S., M.S., and Ph.D. degrees in electrical engineering from the University of Illinois at Urbana-Champaign, Urbana, IL, USA, in 2007, 2009, and 2012, respectively.

He is currently an Associate Professor with the Department of Electrical and Computer Engineering, University of Minnesota, Minneapolis, MN, USA. His research interests include modeling, analysis, and control of power electronics and power systems with a focus on renewable integration.

Dr. Dhople is the recipient of the National Science Foundation CAREER Award in 2015 and the Outstanding Young Engineer Award from the IEEE Power and Energy Society in 2019. He is an Associate Editor for the IEEE TRANSACTIONS ON ENERGY CONVERSION and the IEEE TRANSACTIONS ON POWER SYSTEMS.

Seth R. Sanders (Fellow, IEEE) received the B.S. degree in electrical engineering and physics, and the S.M. and Ph.D. degrees in electrical engineering from the Massachusetts Institute of Technology, Cambridge, MA, USA, in 1981, 1985, and 1989, respectively.

He is Professor with the Department of Electrical Engineering and Computer Sciences at the University of California, Berkeley, VA, USA, and Co-Founder and Chief Scientist at Amber Kinetics, a technology developer and manufacturer of utility scale flywheel energy storage systems. From 1981 to 1983, he was a Design Engineer at the Honeywell Test Instruments Division. In 1989, he joined the UC Berkeley Faculty. From 1992 to 1993, he was on industrial leave with National Semiconductor, Santa Clara, CA, USA. He is currently or has recently been active in supervising research projects in the areas of renewable energy systems, high frequency integrated power conversion circuits, IC designs for power conversion applications, and electric machine systems. His research interests include electrical energy and power conversion systems.

Dr. Sanders is the recipient of the NSF Young Investigator Award and multiple Best Paper Awards from the IEEE Power Electronics and the IEEE Industry Applications Societies. He has served as Chair of the IEEE PELS Technical Committee on Computers in Power Electronics, Chair of the IEEE PELS Technical Committee on Power Conversion Components and Systems, and Member-At-Large of the IEEE PELS Adcom. He is a past Distinguished Lecturer of the IEEE PELS and IAS societies, and recipient of the IEEE PELS Modeling and Control Technical Achievement Award.